

We thank both reviewers for their helpful comments and suggestions. Below we explain how the comments are addressed and make note of changes in the revised manuscript.

Reviewer #1:

The authors performed fine-resolution model simulations using coupled WRF-Chem model to study the individual and combined effect of changes in land use and atmospheric aerosol loading from 1970 to 2006 on the climatic changes. The paper is generally well-written and the results are well discussed. I have following comments before it is accepted to be published on ACP.

One major comment:

1. According to Table 2&3, the authors quantified the urban land use changes on the climatic effect under the atmospheric aerosol loading in 2006, and the aerosol loading changes on the climatic effect under the land use in 1970. Have the authors considered to run extra sensitivity simulation with LU06E70, to quantify these effects under the same year's base condition? How the authors consider the uncertainties associated with that?

Response: We agree with the reviewer that we can also quantify the land cover effect under the aerosol loading in 1970 and the aerosol effect under the land use in 2006 by conducting an additional simulation LU06E70. We carefully thought about this during our experimental design, but we don't expect the land cover effect and the aerosol effect would substantially depend on the background aerosol condition and land use condition, respectively. On the other hand, the multi-year high-resolution WRF-Chem simulation is computationally expensive. It took nearly two wall-clock years to conduct the three experiments, so it wasn't feasible to conduct the additional LU06E70 simulation. The results of aerosol effects by using LU06E06–LU06E70 are likely to be quantitatively different from those using LU70E06–LU70E70, but we believe the differences will not change the qualitative results and major findings/conclusions in this study. The uncertainties in aerosol effect associated with this would not be even comparable to those in aerosol emissions and model physics.

Minor comments:

1. Pg 9: line 178: Can the authors elaborate why they consider the nighttime light correction for deriving the land use data in 2006 but not for 1970?

Response: We didn't use the correction for land use data for 1970 because the nighttime light data started from 1992. So we used the USGS data for 1970 instead. The urban area, which should be very small comparing with 2006, is ignored in 1970 USGS data.

2. Pg 12: line 241-243, the description of the Figure 6 is not the same as in Pg 47. Please double check the imposed surface wind speed is from LU70E70 or LU06E06? Change "PM_{2.5}" to "PM2.5"; Also update the quality of Figure 6. It is less clear compared with other figures.

Response: Thanks for the reviewer's good catch. The imposed surface wind speed is indeed from LU70E70. This has now been corrected in the description of Fig. 6 in the revised manuscript (Line 248). $PM_{2.5}$ has also been changed to PM2.5 as suggested. The quality of Figure 6 has also been much improved in the revised manuscript.

3. Pg 12: line 252: have the authors consider how the different definition of the heatwave could affect the results?

Response: Yes, we did also consider other definitions of heatwave. For instance, according to the definition by WMO, heatwave occurs when the temperature reaches or exceeds $32^{\circ}C$ for 3 consecutive days or more. In this study, the definition we choose is according to the China Meteorological Administration (CMA), which is believed to be more suitable for the regional climate in the Yangtze River Delta Region. Figure R1 illustrates the land cover effect on heatwave days for the two definitions respectively. We can see that the spatial patterns of results for both definitions are quite similar, but there an obvious increase in heatwave days over the major mega cities when the temperature threshold for heatwaves is lower ($32^{\circ}C$ vs. $35^{\circ}C$) as expected. Although the increase in heatwave is greater for the WMO definition, with an average rate of 8.7 d/yr in the major mega cities, the qualitative conclusion doesn't change.

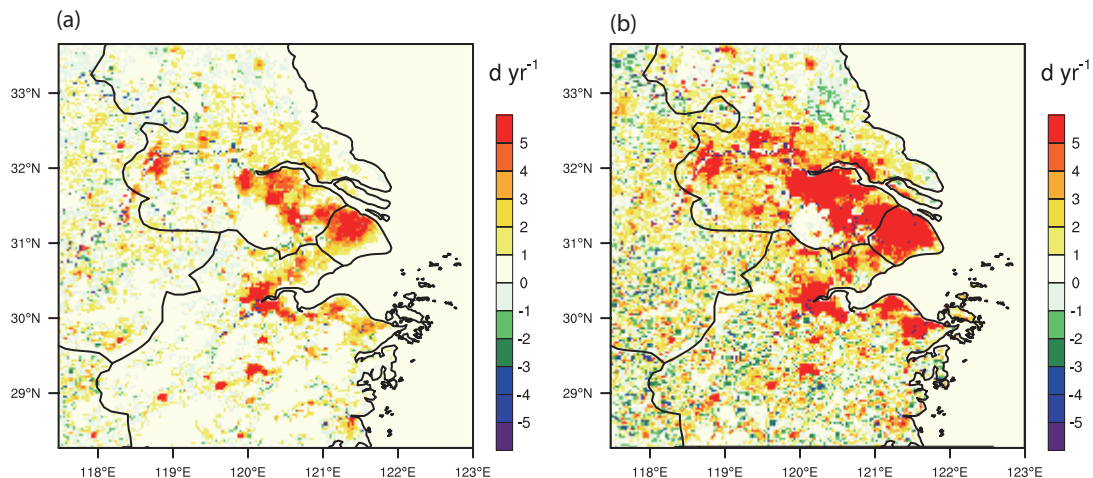


Figure R1 Differences in mean summertime heatwave days (units: d/yr) between LU06E70 and LU70E70 for (a) CMA and (b) WMO definition.

4. Pg 44: figure 3, change "unit" to "units"

Response: Changed it in the revised manuscript.

5. Pg 49: Figure 8: I would suggest the authors to rewrite the captions for Figure 8. Since it no longer shows the subtitle of "Land-Cover" "Aerosol" as in Figures 4 &5, I

think it is better to express that the red lines are for Land cover, blue lines for Aerosol effect, and green lines for total.

Response: [We have made the suggested change for clarity.](#)

6. Pg 51: Figure 10 (a), missing the units of “ 10^{-5} s^{-1} ” in the top of the vertical colorbar.

Response: [Thanks for catching that. The units have been added as suggested.](#)

Reviewer #2:

1. Abstract L38-42: The role of synoptic forcing was not well summarized. These descriptions were too general.

Response: Thanks for the suggestion. In the revised manuscript, we have added a more detailed summary for the role of synoptic forcing (Line 40-46).

2. One issue about the experimental design: the NCEP FNL reanalysis data with 1 degree was directly used to drive the WRF model at 3km. The ratio of the resolution of driving data to that of the regional climate model is about 40, which is quite large. The authors should justify this issue.

Response: The lateral boundary condition is provided to the WRF domain using the NCEP reanalysis data via linear interpolation, so it can represent the horizontal linear variation of meteorological data, no matter how much the ratio of the resolution is. In previous studies that use a regional model to do similar long-term simulations, the NCEP data was also directly used to drive the model at the resolution of less than 10km (e. g. Wang et al., 2015). More importantly, in our model evaluation section, it is shown that the model can generally capture the annual mean climate in the domain.

Wang, X. M., Sun, X. G., Tang, J. P., and Yang, X. Q.: Urbanization-induced regional warming in Yangtze River Delta: potential role of anthropogenic heat release, *Int. J. Climatol.*, doi: 10.1002/joc.4296, 2015.

3. L152: how about the variation from 0800 to 1700? Linearly?

Response: No, it is non-linear. The figure below shows the default diurnal variation of AH in WRF.

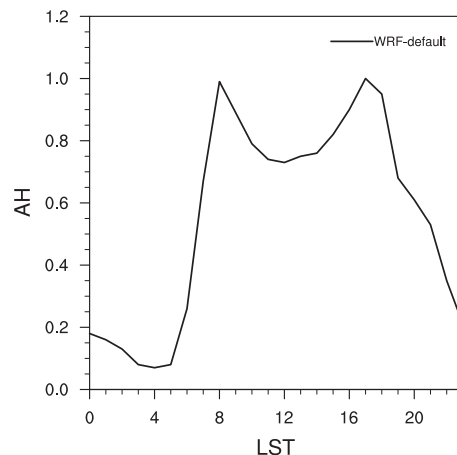


Figure R2 Diurnal cycle of anthropogenic heating (AH) normalized by the peak value of 50 W m⁻² for the WRF default.

4. L198-L207: the authors evaluated the model performance in terms of the annual mean values. However, the changes of summer and winter climate were analyzed respectively in the following sections. So how about the model performance in simulating summer and winter climate?

Response: We have also evaluated the model performance in terms of both summer and winter climate. Fig. R3 illustrates the averaged near-surface temperature and precipitation in summer and winter respectively. The simulated spatial pattern of near-surface air temperature agrees well with observations for both summer and winter, with high temperature centers located at meteorological stations in major cities. The model generally captures the observed precipitation except for the overestimation in summer and the underestimation in winter over the southern part of the domain.

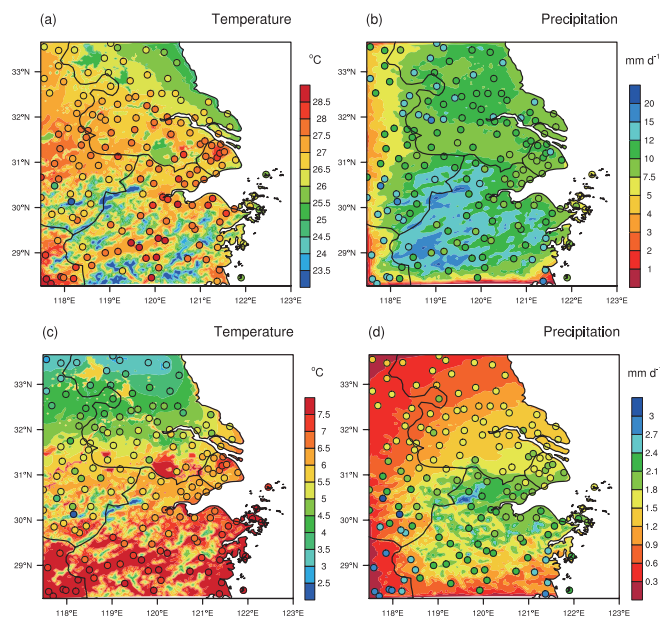


Figure R2 (a) near-surface temperature (units: °C) and (b) precipitation (units: mm d⁻¹) from observations (shaded circles) and simulation of the LU06E06 (shaded) for summer. Panels (c-d) are the same as (a-b) but for winter.

5. Figure 6: the quality of this figure is poor due to its low resolution.

Response: The quality of this figure has been much improved it in the revised manuscript.

6. L403-L412: The authors stated that “the differences in the responses of moisture advection between two cases are related to different background circulation”. I am not very convinced about this argument. In fact, the changes in moisture advection could be further decomposed into three terms, as shown below:

$$-\Delta V \cdot \nabla q = -V_{\text{ctrl}} \cdot \Delta(\nabla q) - (\nabla q)_{\text{ctrl}} \cdot \Delta V - \Delta(\nabla q) \cdot \Delta V$$

$\Delta ()$ represents the difference between the sensitivity and control simulations, and the subscript 'ctrl' denotes the control experiment. The first term in the right-hand side of is associated with the change in water vapor, while the second term is associated with the change in circulation. The third term is a nonlinear term including the contribution of both the moisture and circulation changes. This decomposition could answer whether the background circulation is indeed very important as the authors stated.

Response: Thanks for the suggestion. We have calculated these three terms in the decomposition as suggested. Fig. R3 illustrates time-height cross section of the changes in the first and the second term, respectively. The contribution of the third nonlinear term is small and negligible compared to the other two terms (figure not shown). We can see that the most significant difference between these two cases is the change in the first term, which is directly associated with the background circulation. Therefore, the changes in moisture advection (MA) are much larger in case B due to the stronger background winds. We have used this figure to replace the original Fig. 16 to make our argument more convincing.

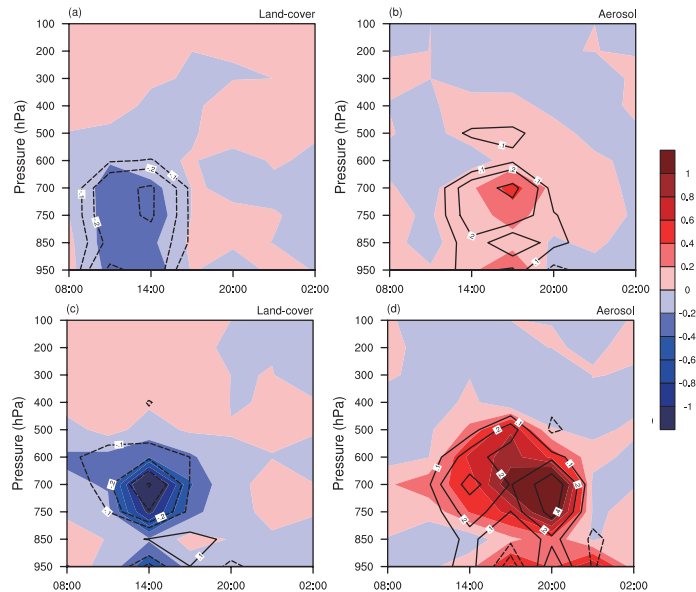


Figure R2 Time-height cross-sections of differences in first term ($-V_{\text{ctrl}} \cdot \Delta(\nabla q)$) (shaded; units: $10^{-4} \text{ g}^{-1} \text{ kg}^{-1} \text{ s}^{-1}$) and second term ($-(\nabla q)_{\text{ctrl}} \cdot \Delta V$) (black lines; units: $10^{-4} \text{ g}^{-1} \text{ kg}^{-1} \text{ s}^{-1}$) for case A over region R1 (denoted in Fig. 12a) between (a) LU06E70 and LU70E70; (b) LU70E06 and LU70E70; Panels (c, d) are the same as (a, b) but for case B over R2 (denoted in Fig. 12d).

1 **Urbanization-induced urban heat island and aerosol effects on**
2 **climate extremes in the Yangtze River Delta Region of China**

3 Shi Zhong^{1,2}, Yun Qian^{2*}, Chun Zhao^{2,6}, Ruby Leung², Hailong Wang², Ben Yang^{3,2}, Jiwen
4 Fan², Huiping Yan^{4,2}, Xiu-Qun Yang³, and Dongqing Liu⁵

5
6 ¹ State Key Laboratory of Hydrology-Water Resources and Hydraulic Engineering, Center for
7 Global Change and Water Cycle, Hohai University, Nanjing, China

8 ² Pacific Northwest National Laboratory, Richland, WA, USA

9 ³ School of Atmospheric Sciences, Nanjing University, Nanjing, China

10 ⁴ College of Atmospheric Science, Nanjing University of Information & Technology, Nanjing,
11 China

12 ⁵ Nanjing Meteorological Bureau, Nanjing, China

13 ⁶ University of Science and Technology of China, Hefei, China

14
15 Corresponding author: Yun Qian [Yun.Qian@pnnl.gov]

16
17 Submitted to *Atmospheric Chemistry and Physics*

18 October 1, 2016

20 **Abstract**

21 The WRF-Chem model coupled with a single-layer Urban Canopy Model (UCM) is
22 integrated for 5 years at convection-permitting scale to investigate the individual and combined
23 impacts of urbanization-induced changes in land cover and pollutants emission on regional
24 climate in the Yangtze River Delta (YRD) region in eastern China. Simulations with the
25 urbanization effects reasonably reproduced the observed features of temperature and
26 precipitation in the YRD region. Urbanization over the YRD induces an Urban Heat Island (UHI)
27 effect, which increases the surface temperature by 0.53 °C in summer and increases the annual
28 heat wave days at a rate of 3.7 d/yr in the major megacities in the YRD, accompanied by
29 intensified heat stress. In winter, the near-surface air temperature increases by approximately 0.7
30 °C over commercial areas in the cities but decreases in the surrounding areas. Radiative effects
31 of aerosols tend to cool the surface air by reducing net shortwave radiation at the surface.
32 Compared to the more localized UHI effect, aerosol effects on solar radiation and temperature
33 influence a much larger area, especially downwind of the city-cluster in the YRD.

34 Results also show that the UHI increases the frequency of extreme summer precipitation
35 by strengthening the convergence and updrafts over urbanized areas in the afternoon, which
36 favor the development of deep convection. In contrast, the radiative forcing of aerosols results in
37 a surface cooling and upper atmospheric heating, which enhances atmospheric stability and
38 suppresses convection. The combined effects of the UHI and aerosols on precipitation depend on
39 synoptic conditions. Two rainfall events under two typical but different synoptic weather patterns
40 are further analyzed. **It is shown that the impact of urban land-cover and aerosols on precipitation
41 is not only determined by their influence on local convergence, but also modulated by large-scale
42 weather systems. For the case with a strong synoptic forcing associated with stronger winds and**

43 larger spatial convergence, the UHI and aerosol effects are relatively weak. When the synoptic
44 forcing is weak, however, the UHI and aerosol effects on local convergence dominate. This
45 suggests that synoptic forcing plays a significant role in modulating the urbanization-induced
46 land-cover and aerosol effects on individual rainfall event. Hence precipitation changes due to
47 urbanization effects may offset each other under different synoptic conditions, resulting in little
48 changes in mean precipitation at longer time scales.

49

50

51

52

53

54

55

56 **1. Introduction**

57 Urbanization affects climate and hydrological cycle by changing land cover and surface
58 albedo, which releases additional heat to the atmosphere, and by emitting air pollutants, which
59 interact with clouds and radiation (e.g., Shepherd, 2005; Sen Roy and Yuan, 2009; Yang et al.,
60 2011). The most discernible impact of urban land-use change is the urban heat island (UHI)
61 effect that can result in a warmer environment over urban areas than the surrounding areas
62 (Landsberg, 1981; Oke, 1987). In addition to the thermal perturbations, the UHI has been well
63 documented to modify wind patterns (Hjemfelt, 1982), evaporation (Wienert and Kuttler, 2005),
64 atmospheric circulations (Shepherd and Burian, 2003; Baik et al., 2007; Lei et al., 2008), and
65 precipitation around urban areas (Braham, 1979; Inoue and Kimura, 2004). Previous studies have
66 found an increase of warm-season precipitation over and downwind of major cities due to the
67 expanded urban land cover (Huff and Changnon, 1972; Changnon, 1979; Zhong et al., 2015).
68 Recent studies suggested that the underlying urban surface also affects the initiation and
69 propagation of storms (Bornstein and Lin, 2000; Guo et al., 2006) and convective activities in
70 city fringes (Baik et al., 2007; Shepherd et al., 2010).

71 Concurrently increases in population and anthropogenic activities over urbanized areas
72 increase pollutant emissions and aerosol loading in the atmosphere. Atmospheric aerosols have
73 long been recognized to affect surface and top of the atmosphere (TOA) radiative fluxes and
74 radiative heating profiles in the atmosphere via aerosol-radiation interactions (ARI) (e.g.,
75 Coakley et al., 1987; Charlson et al., 1992; Hansen et al., 1997; Yu et al., 2006; Qian et al., 2006,
76 2007, 2015; McFarquhar and Wang, 2006), which tend to induce cooling near the surface and
77 heating at the low and mid-troposphere (Qian et al., 2006; Bauer and Mennon, 2012).
78 Anthropogenic aerosols can also affect clouds and precipitation via aerosol-cloud interactions

79 (ACI) (e.g., Rosenfeld, 2000, 2008; Qian et al., 2010; Fan et al., 2013; 2015; Tao et al., 2012;
80 Zhong et al., 2015). Localized changes in precipitation by strong aerosol perturbations can
81 induce cold pools by evaporation, which may alter the organization of stratocumulus clouds (e.g.,
82 Wang and Feingold, 2009; Feingold et al., 2010). Aerosol impacts on deep convective clouds are
83 complicated by the interactions among dynamical, thermodynamical, and microphysical
84 processes. For example, deep convection could be invigorated by aerosols as more cloud water
85 associated with the smaller cloud drops is carried to higher levels where it freezes and releases
86 more latent heat in a polluted environment (Rosenfeld, 2008; Khain, 2009; Storer and van den
87 Heever, 2013). Fan et al. (2013) revealed a microphysical effect of aerosols from reduced fall
88 velocity of ice particles that explains the commonly observed increases in cloud top height and
89 cloud cover in polluted environments. Therefore, urbanization may influence precipitation and
90 circulation through multiple pathways that are more difficult to disentangle than the dominant
91 effect on temperature.

92 As one of the most developed regions in China, the Yangtze River Delta (YRD) has been
93 experiencing rapid economic growth and intensive urbanization process during the past three
94 decades. With the highest city density and urbanization level in China, the YRD has become the
95 largest adjacent metropolitan areas in the world. It covers an area of $9.96 \times 10^4 \text{ km}^2$, with a total
96 urban area of $4.19 \times 10^3 \text{ km}^2$ (Hu et al., 2009). Observations have shown that the urban land-use
97 expansion in this region has induced a remarkable warming due to the significant UHI effect (Du
98 et al., 2006; Wu and Yang 2012, Wang et al., 2015). The annual mean warming reached up to
99 $0.16^\circ\text{C}/10\text{yr}$ based on station measurements in large cities (Ren et al., 2008), which accounted
100 for 47.1% of the overall warming during the period of 1961-2000. Urbanization in the YRD was
101 found to destabilize the atmospheric boundary layer (Zhang et al., 2010) and enhance convection

102 and precipitation (Yang et al., 2012, Wan et al., 2013). Meanwhile, human activities associated
103 with the ever-growing population have led to a dramatic increase in air pollutant emissions
104 (Wang et al., 2006). Several observational and numerical studies have revealed that additional
105 aerosol loading in this region could reduce solar radiation reaching the surface (Che et al., 2005;
106 Qian et al., 2006, 2007), modify warm cloud properties (Jiang et al., 2013), and suppress light
107 rainfall events (Qian et al., 2009).

108 The individual effects of urbanization-induced UHI and aerosol emission on local and
109 regional climate have been examined separately in several modeling studies using short
110 simulations of selected weather episodes at high spatial resolution or multiple-year climate
111 simulations at coarse resolution. To more robustly quantify the urbanization-induced UHI and
112 aerosol effects, convection-permitting simulations may reduce uncertainties in representing
113 convection and its interactions with aerosols, which are parameterized in coarse-resolution
114 models. Additionally, multi-year simulations are needed to understand and quantify the overall
115 effects of land-cover change and aerosols in different large-scale environments (Oleson et al.,
116 2008). In this study, a state-of-the-art regional model coupled with online chemistry (WRF-
117 Chem) and a single-layer Urban Canopy Model (UCM) is used to simulate climate features in
118 the YRD region. The climatic effects of the separate and combined land-cover and aerosol
119 changes induced by urbanization are investigated using a set of 5-year (2006-2010) simulations
120 with a horizontal resolution at convection-permitting scale (3 km). The paper is organized as
121 follows. Section 2 describes the model configuration, experiment design, and model evaluation.
122 The urbanization effects on extreme temperature and precipitation are presented in Section 3,
123 followed by a summary of the conclusions in Section 4.

124

125 **2. Method**

126 **2.1 Model configuration**

127 The WRF-Chem model (Grell et al., 2005; Fast et al., 2006; Qian et al., 2010) simulates
128 trace gases, aerosols and meteorological fields interactively (Skamarock et al., 2008; Wang et al.,
129 2009), including aerosol-radiation interactions (Zhao et al., 2011, 2013a) and aerosol-cloud
130 interactions (Gustafson et al., 2004). The coupled single-layer UCM (Kusaka et al., 2001; Chen
131 et al., 2001) is a column model that uses a simplified geometry with two-dimensional,
132 symmetrical street canyons to represent the momentum and energy exchanges between the urban
133 surface and the atmosphere. The RADM2 (Regional Acid Deposition Model 2) gas chemical
134 mechanism (Stockwell et al., 1990) and the MADE (Modal Aerosol Dynamics Model for
135 Europe) and SORGAM (Secondary Organic Aerosol Model) aerosol module (Schell et al., 2001)
136 are used. Detailed configuration of the above models can be found in Zhao et al. (2010). No
137 cumulus parameterization is used at the convection-permitting resolution. The physical
138 parameterization schemes used in our simulations are listed in Table 1.

139 **2.2 Numerical experiments**

140 Simulations are performed over a model domain centered at (120.50 °E, 31.00 °N) with a
141 horizontal grid spacing of 3 km and 50 vertical levels extending from the surface to 50 hPa. The
142 lowest 10 model layers are placed below 1 km to ensure a fine vertical resolution within the
143 planetary boundary layer. Initial and boundary conditions for meteorological fields are derived
144 from the National Center for Environmental Prediction (NCEP) FNL global reanalysis data on 1°
145 $\times 1^\circ$ grids at 6-hour interval. Lateral boundary conditions for chemistry are provided by a quasi-

146 global WRF-Chem simulation (Zhao et al., 2013b) that includes aerosols transported from
147 regions outside the model domain.

148 The dominant land cover within each model grid cell is derived from the U.S. Geological
149 Survey (USGS) 30 second dataset that includes 24-category land-use type, except that the land
150 use over urban areas is updated using the stable nighttime light product (version 4) at 1 km
151 spatial resolution (available at the National Geophysical Data Center,
152 <http://ngdc.noaa.gov/eog/dmsp/downloadV4composites.html>). Corresponding to the value of
153 lighting index of 25-50, 50-58, and >58 in the above product, each urban grid is identified as
154 “Low Intensity Residential (LIR)”, “High Intensity Residential (HIR)”, or
155 “Commercial/Industrial/Transportation (CIT)”, respectively. Figures 1a and 1b illustrate the
156 urban area within the model domain for year 1970 and 2006, respectively. The anthropogenic
157 heating (AH), characterized by a diurnal cycle with two peaks at rush hours of 0800 and 1700
158 LST, respectively, is incorporated in the model simulations. The default maximum values of AH
159 in WRF for LIR (20 W m^{-2}), HIR (50 W m^{-2}) and CIT (90 W m^{-2}) are used in this study (Tewari
160 et al., 2007). Anthropogenic emissions of aerosols and their precursors are obtained from the
161 Asian emission inventory (Zhang et al., 2009b), which is a $0.5^\circ \times 0.5^\circ$ gridded dataset for 2006.
162 Black carbon (BC), organic matter (OM), and sulfate emissions over China are extracted from
163 the China emission inventory for 2008 (Lu et al., 2011), which provides monthly mean data on
164 $0.1^\circ \times 0.1^\circ$ grids. It should be noted that the Noah land surface model defines a dominant land
165 cover type for each grid, so no subgrid variability is simulated.

166 The anthropogenic emission fluxes of SO_2 and BC in the simulation domain are shown in
167 Figures 1c and 1d, respectively. Areas with large emissions are mainly located in four city
168 clusters, i.e., Nanjing-Zhenjiang-Yangzhou, Suzhou-Wuxi-Changzhou, Shanghai, and Hangzhou

169 Bay, all inside the mega-city belt. Biomass burning emissions for the simulation period are
170 obtained from the monthly Global Fire Emissions Database Version 3 (GFEDv3), which
171 provides monthly mean data on $0.5^\circ \times 0.5^\circ$ grids and the vertical distribution is determined by
172 the injection heights described by Dentener et al. (2006) for the Aerosol Inter-Comparison
173 project (AeroCom). Sea salt and dust emissions are configured following the same approach of
174 Zhao et al. (2013b).

175 In order to investigate the individual responses of local and regional climate to land-cover
176 change and increased aerosol loading, three experiments (i.e., LU06E06, LU70E70, and
177 LU70E06) are conducted for 5 years from 2006 to 2010. The configurations of land use and
178 aerosol emissions for these experiments are summarized in Table 2. All three simulations are
179 performed using the same initial and boundary conditions and physics schemes, but with
180 different land use types and/or anthropogenic emissions. LU06E06 is the control experiment,
181 which represents the “present” (2006) urbanization level for both land use and aerosol/precursor
182 emissions. LU70E06 uses the present aerosol emission data but with the land use of the 1970s,
183 which is derived from the USGS dataset without the nighttime light correction. In LU70E70,
184 both land use and emissions are set to the conditions of the 1970s. The differences of LU06E06-
185 LU70E06, LU70E06-LU70E70, and LU06E06-LU70E70 can be used to derive the urban land-
186 use effect, aerosol effect, and their combined effect, respectively (Table 3). The simulations are
187 initialized on December 15 of each year during 2005-2009 to allow for a 16-day spin-up time
188 and then continuously integrated for the next year (from January 1 to December 31). Results
189 from January 1 to December 31 of all five years (2006-2010) are analyzed.

190 **2.3 Model evaluation**

191 The surface skin temperature simulated in LU06E06 is averaged over 2006-2010 and
192 compared with the MODIS data. A spatial filtering method described by Wu and Yang (2012) is
193 applied to isolate the heterogeneous climatic forcing of urbanization. More specifically, for each
194 grid a spatial anomaly is defined as the departure from the average value over a region centered
195 at each grid. Then, the moving spatial anomalies are calculated for all the grids with the moving
196 region acting as a filtering window, which has a size of $1^\circ \times 1^\circ$. Figure 2 shows the moving
197 spatial anomalies of mean surface skin temperature from MODIS observations and the L06E06
198 simulation. The simulation captures the spatial distribution of observed surface skin temperature
199 very well. In particular, the warmer centers over highly urbanized areas are well reproduced,
200 despite slight underestimations in some mega cities in Zhejiang Province such as Hangzhou and
201 Ningbo. Shanghai and Su-Xi-Chang exhibit the highest temperatures that are 2 °C above the
202 surrounding rural areas.

203 To further validate the model, the baseline simulation LU06E06 is evaluated against
204 meteorological station observations for 2006-2010. Figure 3 shows the averaged near-surface
205 temperature and precipitation from observations and LU06E06. The simulated spatial pattern of
206 near-surface air temperature agrees well with observations, with high temperature centers located
207 at meteorological stations in major cities such as Shanghai and Hangzhou. The simulated
208 temperature displays substantial spatial variability associated with heterogeneity in topography,
209 land cover, and other regional forcings. The model captures the general north-to-south gradient
210 of increasing precipitation in the observations. However, the model overestimates precipitation in
211 Shanghai and central Jiangsu Province but underestimates the precipitation in the southwestern
212 part of the domain.

213

214 **3. Results**

215 **3.1 Urbanization impact on surface temperature, radiation flux and heat waves**

216 **3.1.1 Mean near-surface air temperature**

217 Figure 4 shows the differences in 2-meter near surface air temperature (T2m) among the
218 three experiments to quantify the UHI and aerosol effects from urbanization (Table 3). The UHI
219 effect causes an increase in near-surface temperature over the urbanized area in summer. The
220 average temperature increase is about 0.53 °C over urban area and 1.49 °C in commercial areas
221 outlined by the green contours (see Fig. 4a). In winter, the UHI warming effect occurs primarily
222 in commercial areas, where the mean temperature increases by about 0.7 °C. In areas
223 surrounding the central commercial region, however, temperature decreases due to the urban
224 land-cover change (shown in Fig. 4d). Such a cooling effect in winter has also been found in
225 previous studies (e. g., Oke, 1982; Jauregui et al., 1992; Wang et al., 2007). The “cool island”
226 effects of urbanization during daytime in winter can be explained by the much larger surface
227 thermal inertia of urban areas than that of rural areas with very low vegetation cover during
228 winter (Wang et al., 2007). Although the wintertime cooling effect in urbanized area is not
229 widely recognized, it is an important phenomenon that is also simulated by the model.

230 The increased aerosols induced by urbanization exert a cooling effect over the entire
231 simulation domain in both summer and winter (Fig. 4b and 4e). On a domain average, the
232 temperature reduction induced by increased aerosols is less than the warming induced by the
233 UHI effect in both seasons. Therefore, the net urbanization impact (including both land-cover
234 change and aerosol increase) on near-surface temperature is dominated by the UHI warming
235 effect (Fig. 4c and 4f) resulted from the land-cover change in the YRD.

236 **3.1.2 Surface solar radiation**

237 The effects of urban land-cover change and increased aerosols on surface net shortwave
238 radiation are shown in Fig. 5. As the building clusters reduce surface albedo (Oke, 1987), land-
239 cover change increases the net shortwave radiation over urbanized areas, with an average
240 increase of 9.11 W m^{-2} in summer and 8.49 W m^{-2} in winter. The net increase is greater in
241 summer than in winter because of the stronger summertime incoming solar radiation. On the
242 contrary, aerosols reduce the surface net shortwave radiation in the northern part of the domain
243 corresponding to the larger SO_2 and BC emission rates (Fig. 1), with a magnitude of 8.79 W m^{-2}
244 in summer and 7.63 W m^{-2} in winter. Different from the UHI effect that is more localized, the
245 radiative impact of aerosols is more widespread and significant west of the major urban areas
246 and even over the ocean. Figure 6 shows the spatial pattern of mean surface winds simulated in
247 LU70E06 and the difference in column-integrated PM2.5 mass concentration between
248 LU70E06 and LU70E70. Consistent with the prevailing monsoon circulation, southeasterly
249 (northeasterly) flows dominate the YRD in summer (winter), which lead to increases in the
250 PM2.5 concentration over the downwind area of the YRD city clusters. The increased PM2.5
251 concentrations downwind of the YRD reduce solar radiation to the west (southwest) of the YRD
252 in summer (winter), as shown in Figs. 5b and 5d. Hence aerosol effects on radiation are not
253 limited to the emission source areas in metropolitan regions.

254 **3.1.3 Heat waves**

255 The UHI effect can significantly increase the near-surface temperatures in summer,
256 thereby exacerbating extreme heat waves in urbanized areas (Stone, 2012). By definition, a heat
257 wave occurs when the near-surface temperature reaches or exceeds $35 \text{ }^\circ\text{C}$ for three or more

258 consecutive days (Tan et al., 2004). The averaged heat wave days comparing LU06E06 and
259 LU70E06 increase at a rate of 3.7 d/yr in the major mega cities (Fig. 7a). The increase is most
260 pronounced in Shanghai, with a rate larger than 12 d/yr.

261 High temperature during heat wave contributes to heat exhaustion or heat stroke, but the
262 impact of atmospheric humidity on evaporation is also crucial. Here we use a heat stress index to
263 assess the combined effects of temperature and humidity on human health due to the UHI effect,
264 expressed as (Masterson and Richardson, 1979):

$$265 \quad \text{Humidex} = Ta + (5/9)(e - 10) \quad (1)$$

266 where Ta is near-surface air temperature ($^{\circ}\text{C}$) and e is water vapor pressure (hPa). Figure 7b
267 depicts a big increase in heat stress index (Humidex) over urbanized regions in the YRD, except
268 for the city of Hangzhou. The increase in heat stress index is more accentuated in Shanghai, with
269 a mean increase of 2.16, relative to other urban areas. This suggests that humidity has a larger
270 influence on heat stress in Shanghai because of its proximity to the ocean compared to urban
271 areas further inland. In contrast, increased aerosols have little impact on heat waves (results not
272 shown) because their impacts on near-surface temperature are much weaker (Fig. 4b).

273 **3.2 Urbanization effects on summertime precipitation**

274 **3.2.1 Long-term impact on extreme rainfall**

275 Previous studies have provided evidence of urbanization effect on precipitation
276 distribution in and around urban areas (e.g. Shepherd et al., 2003; Kaufmann et al., 2007; Miao et
277 al., 2010). Several mechanisms have been proposed for the effects of urbanization on
278 precipitation: (1) the UHI effect can destabilize the planetary boundary layer (PBL) and trigger

279 convection; (2) increased surface roughness may enhance atmospheric convergence that favors
280 updrafts; (3) building obstruction tends to bifurcate rainfall systems and delays its propagation;
281 (4) the change in land-cover decreases local evaporation, (5) anthropogenic emissions increase
282 aerosol loading in the atmosphere, with subsequent effects on precipitation through changes in
283 radiation and cloud processes. These mechanisms contribute to positive and negative changes in
284 precipitation, leading to more complicated effects on precipitation than temperature.

285 In this section we analyze the results of the three 5-year simulations to examine the long-
286 term impact of urbanization on precipitation. The results show that influences of both urban land
287 cover and elevated aerosols on annual and seasonal mean precipitation are relatively small (not
288 shown). This may be due to the urbanization effect for different rainfall events offsetting each
289 other, leading to an overall weak effect on a longer time scale (see Section 3.2.2). Here we focus
290 on the frequency of extreme rainfall over the YRD region. Extreme summer rainfall events are
291 defined using hourly precipitation rate that is above 95th percentile at each grid for the period of
292 2006-2010. Figure 8 shows the diurnal cycles of extreme rainfall frequency and urbanization-
293 induced changes in the areas around Nanjing, Shanghai, and Su-Xi-Chang (shown in Fig. 1b).
294 The frequency of hourly extreme rainfall reaches its maximum at around 16:00-17:00 LST over
295 three urban clusters. Urban land-cover change increases the occurrence of extreme precipitation
296 in the afternoon (12:00 to 20:00 LST). The maximum increase in the frequency of extreme
297 hourly rainfall events for Nanjing, Shanghai, and Su-Xi-Chang can reach 0.86%, 1.09%, and
298 0.79%, respectively, with the peak increase occurring in the late afternoon. On the contrary,
299 aerosols exert an opposite impact to substantially reduce the frequency of extreme rainfall in the
300 afternoon by up to 1.05%, 0.75%, and 0.72% for Nanjing, Shanghai, and Su-Xi-Chang,
301 respectively. These impacts are significant compared to the maximum frequency of hourly

302 extreme rainfall of about 10% in each area. However, opposite effects of land-cover and aerosol
303 emission changes result in a small net urbanization effect on extreme precipitation.

304 Because urbanization influences extreme precipitation primarily in the afternoon, we further
305 analyze extreme rainfall events with a focus on the averages from 1200 to 2000 LST. Figure 9
306 shows the substantial increase in extreme precipitation frequency concentrated over the major
307 metropolitan areas in the YRD, with some compensation in the surrounding areas in general.
308 Aerosols, however, reduce the occurrence of extreme precipitation more uniformly in most areas
309 of the domain. The most significant influence of aerosols is found in the northwest part of the
310 domain where aerosol concentrations increase the most downwind of the urban centers (Fig. 6a).
311 Similar to the effects on surface temperature and solar radiation (Figs. 4 and 5), aerosols have a
312 substantial impact on the occurrence of extreme precipitation over a wider area than the effects
313 of urban land-use change.

314 How do changes in land cover and aerosols modulate extreme rainfall frequency? Figure
315 10a shows the diurnal time-height cross section of the impact of urban land-cover (i.e., the
316 difference between LU06E06 and LU70E06) on temperature and divergence averaged over the
317 three city clusters (Nanjing, Shanghai, and Su-Xi-Chang). Air temperature over the urbanized
318 areas increases significantly in the afternoon (from 1200 to 1800 LST) due to the UHI effect. The
319 warming and the increased roughness length in urban areas favor convergence in the lower
320 atmosphere and divergence above. As a result, the mean updraft increases over the urbanized
321 areas in the afternoon (Fig. 10b), which increases cloud water from the lower to middle
322 troposphere in the afternoon. Shortly before noon, there is a small reduction in low clouds, which
323 may be related to the reduced relative humidity due to warmer temperature and/or reduced
324 evaporation from the urban land cover, the so-called urban dry island effect (e.g., Hage, 1975;

325 Wang and Gong, 2009). The increase in cloud water in the afternoon is consistent with the
326 enhanced updrafts. This mechanism potentially explains the increased frequency of extreme
327 precipitation in urban areas in the afternoon (e.g. Craig and Bornstein, 2002; Rozoff et al., 2003;
328 Wan et al., 2013; Zhong and Yang, 2015a, 2015b).

329 To understand the aerosol-induced reduction in extreme rainfall events, we analyze the
330 diurnal cycle of aerosol effect (i.e., the difference LU70E06 and LU70E70) on radiative heating,
331 vertical velocity, and net solar radiation at the surface (Fig. 11). As BC emission rates are
332 relatively high in the YRD region (Fig. 2d), aerosols heat the atmosphere due to absorption of
333 solar radiation during daytime (from 08:00 to 17:00 LST). As a result of absorption and
334 scattering of solar radiation by aerosols, less solar radiation reaches the surface. These changes at
335 the surface and in the atmosphere stabilize the atmosphere and reduce convective intensity in the
336 afternoon (from 14:00 to 20:00 LST), which reduces the frequency of extreme rainfall events
337 (Koren et al., 2004; Qian et al., 2006; Zhao et al., 2006; 2011; Fan et al., 2007). Although
338 aerosols can enhance precipitation through cloud microphysical changes that invigorate
339 convection (e.g., Khain et al., 2009; Rosenfeld et al., 2008; Fan et al., 2013), aerosol radiative
340 effects generally dominate in China because of the high AOD and strong light-absorbing aerosol
341 properties (Yang et al., 2011; Fan et al., 2015).

342 **3.2.2 Synoptic influence on urbanization impacts**

343 The impacts of urbanization-induced UHI and aerosols on precipitation may be highly
344 variable under different synoptic conditions that influence the atmospheric circulation and cloud
345 and boundary layer processes. Precipitation changes due to urbanization effects may offset each
346 other under different synoptic conditions, leading to an overall weak effect on mean precipitation

347 at longer time scales as discussed in section 3.2.1. We select two typical heavy late-afternoon
348 rainfall events with different background circulations over the YRD region. Case A occurred
349 from 08:00 LST 23 June to 08:00 LST 24 June 2006 and case B occurred from 08:00 LST 1 July
350 to 08:00 LST 2 July 2006. Figure 12a and 12d show the mean precipitation rate and 850 hPa
351 winds for case A and case B, respectively. Southwesterly flow dominates the entire region in case
352 A (Fig. 12a), while in case B (Fig. 12d) southwesterly and northwesterly winds dominate the
353 southern and northern parts of precipitation area, respectively. The averaged background wind
354 speed in case B is much stronger than that in case A, representing stronger synoptic forcing in
355 case B. The effects of urban land-cover change and aerosols on precipitation for the case A (case
356 B) are illustrated in Figs. 12b and 12c (Figs. 12e and 12f), respectively. Both cases show
357 significant precipitation responses to the forcing of urban land-cover and aerosols. We can see
358 that urban land cover increases the rainfall intensity in case A but aerosols decrease precipitation
359 over the urbanized area (Figs. 12b and 12c). The precipitation response to urban land cover and
360 aerosols is just the opposite in case B (Figs. 12e and 12f). Figs. 13a and 13d illustrate the
361 evolution of precipitation in region R1 (Fig. 12a) and R2 (Fig. 12d), respectively, for the two
362 cases. In both cases, rainfall mainly occurred between 08:00 LST and 20:00 LST. The
363 corresponding impacts of urban land-cover and aerosols are shown in Figs. 13b-c and Figs. 13e-f
364 for cases A and B, respectively. In case A, the urban land-cover substantially increases the
365 precipitation intensity in the afternoon with a maximum increase of 6.87 mm h^{-1} . Aerosol effects,
366 on the contrary, decrease the rainfall intensity with a maximum reduction of 3.85 mm h^{-1} . In case
367 B, however, effects of urban land-cover and enhanced aerosols on precipitation are opposite to
368 that in case A. A maximum rainfall reduction of 3.81 mm h^{-1} is found to be associated with the
369 effect of urban land cover and an increase of 2.85 mm h^{-1} is associated with the aerosol forcing.

370 Why do urban land-cover and aerosols exert opposite effects on precipitation during the
371 two rainfall events? Here we attempt to answer this question by examining the dynamical and
372 thermodynamical changes induced by the UHI and aerosols using the moisture flux convergence
373 (MFC), which is defined as:

$$374 \quad \text{MFC} = -\nabla \cdot (q\vec{V}_h) = -q\nabla \cdot \vec{V}_h - \vec{V}_h \cdot \nabla q \quad (2)$$

375 The first and second terms on the right hand side of Eq. 2 denote wind convergence (CON) and
376 moisture advection (MA), respectively.

377 Figures 14a and 14b illustrate the time-height cross sections of changes in moisture flux
378 convergence and cloud water mixing ratio induced by land-cover and aerosol changes over the
379 region R1 (Fig. 12a) during the rainy period in case A. Urban land-cover enhances the
380 convergence of moisture fluxes in the lower troposphere, which results in increased precipitation
381 (Fig. 14a). On the contrary, aerosols weaken the convergence of moisture fluxes and thus reduce
382 precipitation (Fig. 14b). These changes are consistent with those associated with extreme rainfall
383 changes shown in Fig. 10. Interestingly for case B over R2, urban land-cover weakens the
384 convergence of moisture fluxes (Fig. 14c) and thus suppresses precipitation (Fig. 13e) from
385 08:00 LST 1 July to 02:00 LST 2 July 2006. Aerosols, however, enhance the convergence of
386 moisture fluxes over R2 (Fig. 14d) and thus increase precipitation (Fig. 13f). These results
387 establish obvious correspondence between moisture flux convergence changes and the
388 precipitation response to urban land cover and aerosols in the two rainfall events and suggest
389 different processes may dominate the moisture flux convergence changes for the two cases.

390 Figure 15 presents the time-height cross section of the changes in the two terms of MFC,
391 i.e., CON (convergence) and MA (moisture advection), induced by land-cover and aerosol

392 changes averaged over R1 (Fig. 12a) for case A and over R2 (Fig. 12d) for case B. Urban land-
 393 cover enhances the wind convergence over R1 in case A (Fig. 15a), leading to an increase in
 394 CON by up to $1.56 \times 10^{-4} \text{ g kg}^{-1} \text{ s}^{-1}$, which is much larger than the increase of $0.61 \times 10^{-4} \text{ g kg}^{-1} \text{ s}^{-1}$
 395 averaged over R2 (Fig. 15c) in case B. The larger enhancement of convergence in case A is
 396 attributed to the strong UHI-induced surface heating during this rainfall period (figure not
 397 shown). In contrast, aerosols reduce the convergence in both case A and case B due to the aerosol
 398 cooling effect near the surface, as discussed previously (Fig. 11). The reduction of convergence
 399 in case A is more significant than that in case B because of the larger aerosol loading and,
 400 therefore, stronger surface cooling over R1 in case A (not shown). Urban land-cover reduces
 401 moisture advection in both cases, with a maximum decrease of -0.99 and $-1.89 \times 10^{-4} \text{ g kg}^{-1} \text{ s}^{-1}$,
 402 respectively. Aerosols, however, increase moisture advection, and the maximum increases are
 403 0.93 and $1.31 \times 10^{-4} \text{ g kg}^{-1} \text{ s}^{-1}$ in case A and case B, respectively. Our results show clearly that the
 404 changes in CON are opposite to that in MA. As the impacts of urban land-cover and aerosols on
 405 moisture advection are greater in case B than in case A, the net changes in the moisture flux
 406 convergence are dominated by MA in case B and by CON in case A, leading to opposite effects
 407 between the two cases.

408 The significant differences in the responses of MA between the two cases are related to
 409 different background circulations during the two events (Figs. 12a and 12d). Weaker
 410 southwesterly flow dominates the entire region in case A (Fig. 12a), while in case B (Fig. 12d)
 411 stronger southwesterly and northwesterly winds dominate the southern and northern parts of
 412 precipitation area, respectively. The changes in MA could be further decomposed into three
 413 terms, as shown below in Eq. 3:

$$-\Delta \mathbf{V} \cdot \nabla \mathbf{q} = -\mathbf{V}_{\text{ctrl}} \cdot \Delta(\nabla \mathbf{q}) - (\nabla \mathbf{q})_{\text{ctrl}} \cdot \Delta \mathbf{V} - \Delta(\nabla \mathbf{q}) \cdot \Delta \mathbf{V} \quad (3)$$

Formatted: Font color: Red

415 The first term on the right-hand side of is associated with the change in water vapor,
416 while the second term is associated with the change in circulation. The third term is a nonlinear
417 term including the contribution of both the moisture and circulation changes. Figure 16 illustrates
418 the changes in the first and second term, respectively. The contribution of the third nonlinear
419 term is small and negligible compared to the other two terms (not shown). Urban land-cover
420 reduces the first term in both cases, with a maximum decrease of -0.34 and $-1.54 \cdot 10^{-4} \text{g kg}^{-1} \text{s}^{-1}$,
421 respectively. Aerosols, however, increase the first term, and the maximum increases are 0.49 and
422 $1.78 \cdot 10^{-4} \text{g kg}^{-1} \text{s}^{-1}$ in case A and case B, respectively. The urban land-cover and aerosol effects on
423 the second term are quite similar for both cases. Therefore, the most significant difference
424 between these two cases is the change in the first term, which is directly associated with the
425 background circulation. These changes in the first term are much larger in case B because of the
426 stronger background winds than in case A, contributing to a more significant modification in MA
427 as shown in Figure 15.

428 In summary, case B represents stronger synoptic forcing than case A. The stronger winds
429 and larger spatial coverage of clouds and precipitation associated with the larger scale synoptic
430 system weakens the UHI and aerosol effects through ventilation and changes in radiation,
431 resulting in weaker CON and larger MA changes. Conversely, with weaker synoptic forcing, the
432 stronger UHI and aerosol effects enhance the changes in CON while MA effects are smaller due
433 to the weaker background winds. Therefore, our results highlight the distinguishing role of
434 synoptic forcing on how urban land-cover and aerosol influence the dynamical and thermo-
435 dynamical environments and precipitation.

436 **4. Summary**

437 In this study, the state-of-the-art WRF-Chem model coupled with a single-layer UCM, is
438 run at convection-permitting scale to investigate the influences of urbanization-induced land-
439 cover change and elevated aerosol concentrations on local and regional climate in the Yangtze
440 River Delta (YRD) in China. A 5-year period (2006-2010) is selected for multi-year simulations
441 to investigate urbanization effects on extreme events and the role of synoptic forcing. Three
442 experiments were conducted with different configurations of land cover and aerosol emissions:
443 (1) urban land and emissions in 2006, (2) urban land in the 1970s and emissions in 2006, and (3)
444 urban land and emissions in the 1970s. The experiment with the 2006 land-use type and
445 anthropogenic emissions reproduces the observed spatial patterns of near-surface air temperature
446 and precipitation fairly well.

447 The expanded urban land cover and increased aerosols have opposite impacts on the near-
448 surface air temperature. The urban land-use change increases 2-m air temperature due to the UHI
449 effect in commercial areas with a domain-averaged increase of 1.49 °C in summer and 0.7 °C in
450 winter. In the surrounding areas, however, surface air temperature increases in summer but
451 decreases in winter. The latter is attributed to the much greater thermal inertia over urban areas
452 than over rural areas in wintertime when both vegetation cover and soil moisture are at their
453 seasonal minimum. Compared to the effect of land-cover change, aerosol effect exerts a less
454 significant influence on near-surface temperature with minor decreases in both summer and
455 winter. Overall, the impact of urban land-use change outweighs that of enhanced aerosols on
456 regional temperature especially in summer. The increase in near-surface temperature induced by
457 the UHI effect leads to an increase in heat wave days by 3.7 days per year over the major mega
458 cities in the YRD region. The greater response of solar radiation to urban land-cover in summer
459 is the major factor contributing to the larger changes in surface temperature in summer than in

460 winter. Compared to the urban land-use effect, aerosol effect on reducing the surface solar
461 radiation occurs over a much broader region including the downwind area of the city clusters.

462 The urban land-cover change and increased aerosols have opposite effects on the
463 frequency of extreme rainfall during summer. The UHI effect leads to more frequent extreme
464 precipitation over the urbanized area in the afternoon because of an enhanced near-surface
465 convergence and vertical motion. In contrast, aerosol tends to decrease the frequency of extreme
466 precipitation because of its cooling effect near the surface and heating effect (by light-absorbing
467 particles) above, leading to an increased atmospheric stability and weakened updrafts. Additional
468 aerosols can also induce decreases in the frequency of extreme precipitation over non-urban
469 areas, particularly in the downwind area of the city clusters.

470 The effects of both urban land-cover and increased aerosols on summertime rainfall vary
471 with synoptic weather systems and environmental conditions. Two late-afternoon rainfall events
472 are selected for in-depth analysis. For the two cases, urbanization exerts similar impacts on local-
473 scale convergence and mean wind speed, which modify the strength of moisture transport. More
474 specifically, the effect of urban land-cover increases local-scale convergence due to the UHI-
475 induced circulation and reduces low-level wind speed, while aerosols have an opposite effect due
476 to the cooling near the surface. We found that the impacts of urban land-cover and aerosol on
477 precipitation are determined not only by their effect on local-scale convergence, but also
478 modulated by the large-scale weather systems. Our analyses suggest that synoptic forcing plays a
479 significant role in how urbanization-induced land-cover and aerosols influence individual rainfall
480 event. Although the two rainfall events selected for the analysis do not represent all types of
481 precipitation events in the YRD Region, they demonstrate how the effect of urbanization on
482 precipitation may vary and offset each other under different synoptic conditions, leading to an

483 overall weak effect on mean precipitation at longer time scales. To further quantify urbanization
484 effects, uncertainties in anthropogenic emissions and heating, unresolved urban building and
485 streets structure, and representation in aerosol-cloud interactions and cloud microphysics in the
486 model should be investigated in future studies. Further investigation is also needed to have a
487 better and more comprehensive understanding of the complicated mechanisms through which
488 urbanization influences heavy rainfall under a full range of weather conditions.

489
490 **Acknowledgments**

491 The contributions of PNNL authors are supported by the U.S. Department of Energy's
492 Office of Science as part of the Regional and Global Climate Modeling Program and
493 Atmospheric System Research (ASR) program. The contribution of Shi Zhong and Xiu-Qun
494 Yang is supported by the National Basic Research Program of China (2010CB428504), Jiangsu
495 Collaborative Innovation Center for Climate Change, and the Scholarship Award for Excellent
496 Doctoral Student granted by China Scholarship Council. The work of Ben Yang is supported by
497 the National Natural Science Foundation of China (41305084). Computations were performed
498 using resources of the National Energy Research Scientific Computing Center (NERSC) at
499 Lawrence Berkeley National Laboratory and PNNL Institutional Computing. The Pacific
500 Northwest National Laboratory is operated for DOE by Battelle Memorial Institute under
501 contract DE-AC05-76RL01830. All model results are archived on a PNNL cluster and available
502 upon request. Please contact Yun Qian (yun.qian@pnnl.gov).

503

504

505

506

507

508

509 **Reference**

- 510 Baik, J. J., Kim, Y. H., Kim, J. J., and Han, J. Y.: Effect of boundary-layer stability on urban
511 heat island induced circulation, *Theor. Appl. Climatol.*, 89, 73–81, 2007.
- 512 Bauer, S. E., and Menon, S.: Aerosol direct, indirect, semidirect, and surface albedo effects from
513 sector contributions based on the IPCC AR5 emissions for preindustrial and present-day
514 conditions, *J. Geophys. Res.*, 117, D01206, doi: 10.1029/2011JD016816, 2012.
- 515 Bornstein, R., and Lin, Q.: Urban heat islands and summertime convective thunderstorms in
516 Atlanta: Three cases studies, *Atmos. Environ.*, 34, 507–516, 2000.
- 517 Braham, R. R.: Comments on “Urban, topographic and diurnal effects on rainfall in the St. Louis
518 region”. *J. Appl. Meteorol.*, 18, 371-374, 1979.
- 519 Changnon, S. R.: Rainfall changes in summer caused by St. Louis, *Science*, 205, 402–404, 1979.
- 520 Charlson, R. J., et al.: Climate forcing by anthropogenic aerosols, *Science*, 255, 423–430, 1992.
- 521 Che, H. Z., Shi, G. Y., Zhang, X. Y., Arimoto, R., Zhao, J. Q., Xu, L., Wang, B., and Chen, Z. H.:
522 Analysis of 40 years of solar radiation data from China, 1961–2000, *Geophys. Res. Lett.*,
523 32, L06803, doi:10.1029/2004GL022322, 2005.
- 524 Chen, F., Kusaka, H., Bornstein, R., et al.: The integrated WRF/urban modeling system:
525 development, evaluation, and applications to urban environmental problems, *Int. J.*
526 *Climatol.*, 31(2), 273-288, 2001.
- 527 Coakley, J. A., Bernstein, R. L., and Durkee, P. A.: Effect of ship-track effluents on cloud
528 reflectivity, *Science*, 273, 1020–1022, 1987.

529 Craig, K., and Bornstein, R.: MM5 simulation of urban induced convective precipitation over
530 Atlanta. Preprints, Fourth Conf. on the Urban Environment, Norfolk, VA, Amer. Meteor.
531 Soc., 5–6, 2002.

532 Dentener, F., et al.: Emissions of primary aerosol and precursor gases in the years 2000 and 1750
533 prescribed data-sets for AeroCom, Atmos. Chem. Phys., 6, 4321–4344, doi:10.5194/acp-6-
534 4321-2006, 2006.

535 Du, Y., et al.: Impact of urban expansion on regional temperature change in the Yangtze River
536 Delta, J. of Geophys. Sci., 17(4): 387-398, 2006.

537 Fast, J. D, et al.: Evolution of ozone, particulates, and aerosol direct forcing in an urban area
538 using a new fully-coupled meteorology, chemistry, and aerosol model, J. Geophys. Res.,
539 111, D21305, doi:10.1029/2005JD006721, 2006.

540 Fan, J., Leung, L. R., Rosenfeld, D., Chen, Q., Li, Z., Zhang, J., and Yan, H.: Microphysical
541 Effects Determine Macrophysical Response for Aerosol Impacts on Deep Convective
542 Clouds, Proceedings of the National Academy of Sciences of the United States of America,
543 110(48), E4581-E4590, doi:10.1073/pnas.1316830110, 2013.

544 Fan, J., Rosenfeld, D., Yang, Y., Zhao, C., Leung, Y. R., and Li, Z.: Substantial Contribution of
545 Anthropogenic Air Pollution to Catastrophic Floods in Southwest China, Geophys. Res.
546 Lett., 42(14), 6066-6075, doi:10.1002/2015GL064479, 2015.

547 Fan, J., Zhang, R., Li, G., Tao, W., and Li, X.: Simulations of cumulus clouds using a spectral
548 microphysics cloud resolving model, J. Geophys. Res., 112, D04201,
549 doi:10.1175/2010JAS3651.1, 2007.

550 Feingold G., Koren, I., Wang, H., Xue, H., and Brewer W.: Precipitation-generated oscillations in
551 open cellular cloud fields. *Nature*, 466, 849–852, 2010.

552 Grell, G. A., Peckham, S. E., Schmitz, R., et al.: Fully coupled “online” chemistry within the
553 WRF model, *Atmos. Environ.*, 39, 6957–6975, 2005.

554 Gustafson, W. I., Chapman, E. G., Ghan, S. J., Easter, R. C., and Fast, J. D.: Impact on modeled
555 cloud characteristics due to simplified treatment of uniform cloud condensation nuclei
556 during NEAQS 2004, *Geophys. Res. Lett.*, 34, L19809 doi:10.1029/2007GL0300321,2007.

557 Guo, X., Fu, D., and Wang, J.: Mesoscale convective precipitation system modified by
558 urbanization in Beijing city, *Atmos. Res.*, 82, 112–126, 2006.

559 Hage, K. D.: Urban-rural humidity difference, *J. Appl. Meteor.*, 14(7), 1277-1283, 1975.

560 Hansen, J., Sato, M., and Ruedy, R.: Radiative Forcing and Climate Response, *J. Geophys. Res.*,
561 102, 6831–6864, 1997.

562 Hjermfelt, M. R.: Numerical simulation of the effects of St. Louis on mesoscale boundary layer
563 airflow and vertical motion: Simulations of urban vs. non-urban effects, *J. Appl. Meteor.*,
564 21, 1239–1257, 1982.

565 Hu, Y., Ban, Y., Zhang, Q., and Liu, J.: The trajectory of urbanization process in the Yangtze
566 River Delta during 1990 to 2005. 7th Urban Remote Sensing Joint Event, 20–22 May 2009,
567 Shanghai, DOI: 10.1109/URS.2009.5137536, 2009.

568 Huff, F. A., and Changnon Jr., S. A.: Climatological assessment of urban effects on precipitation
569 at St. Louis, *J. Appl. Meteorol.*, 11, 823-842, 1972.

570 Inoue, T., and Kimura, F.: Urban effects on low-level clouds around the Tokyo metropolitan area
571 on clear summer days, *Geophys. Res. Lett.*, 31, L05103, doi:10.1029/2003GL018908, 2004.

572 Jauregui, E., Godinez, L., and Cruz, F.: Aspects of Heat-Island Development in Guadalajara,
573 Mexico, *Atmos. Environ.* 26B, 391–396, 1992.

574 Jiang Y, Liu, X., Yang, X. Q.: A numerical study of the effect of different aerosol types on East
575 Asian summer clouds and precipitation, *Atmos. Environ.*, 70, 51-63, 2013.

576 Kaufmann, R. K., Seto, K. C., Schneider, A., Liu, Z., Zhou, L., Wang, W.: Climate response to
577 rapid urban growth: evidence of a human-induced precipitation deficit, *J. Climate*, 20(10),
578 2299-2306, 2007.

579 Khain A. P.: Notes on state-of-the-art investigations of aerosol effects on precipitation: a critical
580 review, *Environ. Res. Lett.*, 4(1), 015004, 2009.

581 Koren, I., et al.: Measurement of the effect of Amazon smoke on inhibition of cloud formation,
582 *Science*, 303(5662), 1342-1345, 2004.

583 Kusaka, H., Kikegawa, Y., and Kimura, F.: A simple single layer urban canopy model for
584 atmospheric models: comparison with multi-layer and slab models, *Bound-Layer Meteor.*,
585 101, 329–358, 2001.

586 Landsberg, H. E.: *The Urban Climate*, Academic Press, London, UK, 1981.

587 Lei, M., et al.: Effect of explicit urban land surface representation on the simulation of the 26
588 July 2005 heavy rain event over Mumbai, India, *Atmos. Chem. Phys.*, 8 (20), 5975-5995,
589 2008.

590 Lu, Z., Zhang, Q., and Streets, D. G.: Sulfur dioxide and primary carbonaceous aerosol
591 emissions in China and India, 1996–2010, *Atmos. Chem. Phys.*, 11(18), 9839-9864, 2011.

592 Masterson, J., Richardson F. A.: *Humidex. A method of quantifying human discomfort due to*
593 *excessive heat and humidity*, Environment Canada, Downsview, 1979.

594 McFarquhar, G. M., and H. Wang: Effects of aerosols on trade wind cumuli over the Indian
595 Ocean: Model simulations, *Q. J. R. Meteorol. Soc.*, 132, 821–843, 2006.

596 Miao, S. G., Chen, F., Li, Q. C., and Fan, S. Y.: Impacts of urban processes and urbanization on
597 summer precipitation: a case study of heavy rainfall in Beijing on 1 August 2006, *J. Appl.*
598 *Meteorol. Climatol.*, 50, 806–825, 2010.

599 Monin, A. S., and Obukhov, A. M.: Basic laws of turbulent mixing in the surface layer of the
600 atmosphere, *Contributions of the Geophysical Institute of the Slovak Academy of*
601 *Sciences*, 24, 151, 163–187, 1954.

602 Oke, T. R.: The Energetic Basis of the Urban Heat Island, *Q. J. R. Met. Soc.*, 108, 1–22, 1982.

603 Oke, T. R.: *Boundary Layer Climates*. 2d ed. Methuen Co., 435 pp, 1987.

604 Oleson, K. W., Bonan, G. B., Feddema, J., and Vertensten, M.: An urban parameterization for a
605 global climate model. Part II: Sensitivity to input parameters and the simulated urban heat
606 island in offline simulations, *J. Appl. Meteor. Climatol.*, 47, 1061-1076, 2008.

607 Qian, Y., Kaiser, D. P., Leung, L. R., and Xu, M.: More frequent cloud-free sky and less surface
608 solar radiation in China from 1955 to 2000, *Geophys. Res. Lett.*, 33, L01812,
609 doi:10.1029/2005GL024586, 2006.

610 Qian, Y., Wang, W., Leung, L. R., and Kaiser, D. P.: Variability of solar radiation under cloud-
611 free skies in China: The role of aerosols, *Geophys. Res. Lett.*, 34, L12804,
612 doi:10.1029/2006GL028800, 2007.

613 Qian, Y., Gong, D., Fan, J., Leung, L. R., Bennartz, R., Chen, D., Wang, W.: Heavy pollution
614 suppresses light rain in China: Observations and modeling, *J. Geophys. Res.*, 114, D00K02,
615 doi:10.1029/2008JD011575, 2009.

616 Qian, Y., Gustafson Jr, W. I., and Fast, J. D.: An investigation of the sub-grid variability of trace
617 gases and aerosols for global climate modeling, *Atmos. Chem. Phys.*, 10, 6917-6946,
618 doi:10.5194/acp-10-6917-2010, 2010.

619 Qian, Y., Teppe, J., Yasunari, J., et al.: Light-absorbing particles in snow and ice: Measurement
620 and modeling of climatic and hydrological impact. *Adv. Atmos. Sci.*, 32(1), 64–91, doi:
621 10.1007/s00376-014-0010-0, 2015.

622 Ren, G., Zhou, Y., Chu, Z., Zhou, J., Zhang, A., Guo, J., Liu, X.: Urbanization Effects on
623 Observed Surface Air Temperature Trends in North China, *J. Climate*, 21 (6), 1333-1348,
624 2008.

625 Rosenfeld, D.: Suppression of rain and snow by urban and industrial air pollution, *Science*, 287
626 (5459), 1793-1796, 2000.

627 Rosenfeld, D., et al.: Flood or drought: How do aerosols affect precipitation? *Science*, 321,
628 1309–1313, doi:10.1126/science.1160606, 2008.

629 Rozoff, C., Cotton, W. R., and Adegoke, J. O.: Simulation of St. Louis, Missouri, land use
630 impacts on thunderstorms, *J. Appl. Meteor.*, 42, 716–738, 2003.

631 Schell, B., Ackermann, I. J., Hass, H., Binkowski, F. S., and Ebel, A.: Modeling the formation of
632 secondary organic aerosol within a comprehensive air quality modeling system, *J. Geophys.*
633 *Res.*, 106, 28275–28293, 2001.

634 Sen Roy, S., and Yuan, F.: Trends in extreme temperatures in relation to urbanization in the Twin
635 Cities Metropolitan Area, Minnesota. *J. Appl. Meteor.*, 48 (3), 669-679, 2009.

636 Shepherd, J. M., and Burian, S. J.: Detection of urban-induced rainfall anomalies in a major
637 coastal city, *Earth Interactions*, 7(4), 1-17, 2003.

638 Shepherd, J. M., Carter, M., Manyin, M., Messen, D., and Burian, S.: The impact of urbanization
639 on current and future coastal precipitation: a case study for Houston, *Environ. Plan.*, 37,
640 284-304, 2010.

641 Shepherd, J. M.: A review of current investigations of urban-induced rainfall and
642 recommendations for the future, *Earth Interact.*, 9 (12), 1-27, 2005.

643 Skamarock, W. C., Klemp, J. B.: A time-split nonhydrostatic atmospheric model for weather
644 research and forecasting applications, *J. Computational Physics*, 227(7): 3465-3485,
645 2008.

646 Stone, B.: *The city and the coming climate: Climate change in the places we live*, Cambridge
647 University Press, New York, 2012.

648 Stockwell, W. R., Middleton, P., Chang, J. S., and Tang, X.: The second generation regional acid
649 deposition model chemical mechanism for regional air quality modeling, *J. Geophys. Res.*,
650 95, 16343–16367, 1990.

651 Storer R. L., and Van den Heever, S. C.: Microphysical processes evident in aerosol forcing of
652 tropical deep convective clouds, *J. Atmos. Sci.*, 70(2), 430-446, 2013.

653 Tan J., Kalkstein, L. S., Huang, J., Lin, S., Yin, H., Shao, D.: An operational heat/health warning
654 system in Shanghai, *International Journal of Biometeorology*, 48(3), 157-162, 2004.

655 Tao, W. K., Chen, J. P., Li, Z., Wang, C., Zhang, C.: Impact of aerosols on convective clouds and
656 precipitation, *Rev. Geophys.*, 50 (2), 2012.

657 Tewari, M., Chen, F., Kusaka, H., and Miao, S.: Coupled WRF/Unified Noah/urban-canopy
658 modeling system, NCAR WRF Documentation. Boulder: NCAR, 1-20, 2007.

659 Wan, H. C., Zhong, Z., Yang, X. Q., and Li, X. Q.: Impact of city belt in Yangtze River Delta in
660 China on a precipitation process in summer: A case study, *Atmos. Res.*, 125-126, 63–75,
661 2013.

662 Wang, H., and Feingold, G.: Modeling mesoscale cellular structures and drizzle in marine
663 stratocumulus. Part II: The Microphysics and Dynamics of the Boundary Region between
664 Open and Closed Cells, *J. Atmos. Sci.*, 66, 3257–3275, 2009.

665 Wang, H., Skamarock, W. C., and Feingold, G.: Evaluation of scalar advection schemes in the
666 Advanced Research WRF model using large-eddy simulations of aerosol–cloud
667 interactions, *Mon. Wea. Rev.*, **137**, 2547–2558, 2009.

668 Wang, X. Q., and Gong, Y. B.: The impact of an urban dry island on the summer heat wave and
669 sultry weather in Beijing City, *Chinese Science Bulletin*, 55(16), 1657-1661, 2010.

670 Wang, Y., Zhuang, G., Zhang, X., Huang, K., Xu, C., Tang, A., Chen, J., An, Z.: The ion
671 chemistry, seasonal cycle, and sources of PM_{2.5} and TSP aerosol in Shanghai, *Atmos.*
672 *Environ.*, 40(16), 2935-2952, 2006.

673 Wang, K. C., Wang, J., Wang, P., Sparrow, M., Yang, J., Chen, H.: Influences of urbanization on
674 surface characteristics as derived from the Moderate-Resolution Imaging
675 Spectroradiometer: A case study for the Beijing metropolitan area, *J. Geophys. Res.*, 112.
676 D22S06, 2007.

677 Wang, X. M., Sun, X. G., Tang, J. P., and Yang, X. Q.: Urbanization-induced regional warming in
678 Yangtze River Delta: potential role of anthropogenic heat release, *Int. J. Climatol.*, doi:
679 10.1002/joc.4296, 2015.

680 Wienert, U., and Kuttler, W.: The dependence of the urban heat island intensity on latitude—a
681 statistical approach, *Meteorologische Zeitschrift*, 14(5), 677-686, 2005.

682 Wu, Kai, and Yang, X. Q.: Urbanization and heterogeneous surface warming in eastern China,
683 *Chinese Science Bulletin*, 58 (12), 1363-1373, 2013.

684 Yang, Ben, Zhang, Y. C., and Qian, Y.: Simulation of urban climate with high-resolution WRF
685 model: A case study in Nanjing, China, *Asia-Pacific J. Atmos. Sci.*, 48 (3), 227-241, 2012.

686 Yang, X., Hou, Y., Chen, B.: Observed surface warming induced by urbanization in east China, *J.*
687 *Geophys. Res.*, 116 (D14), 2011.

688 Yu, H., Kaufman, Y. J., Chin, M., et al.: A review of measurement-based assessments of the
689 aerosol direct radiative effect and forcing, *Atmos. Chem. Phys.*, 6 (3), 613-666, 2006.

690 Zhang, N., Gao, Z., Wang, X., Chen, Y.: Modeling the impact of urbanization on the local and
691 regional climate in Yangtze River Delta, China, *Theor. Appl. Climatol.*, 102(3-4): 331-342,
692 2010.

693 Zhang, Q., Hu, Y., Liu, J.: The trajectories of urban land and industrial land in Shanghai over the
694 past 30 years, *Urban Remote Sensing Event, 2009 Joint. IEEE*, 2009a.

695 Zhang, Q., Streets, D. G., Carmichael, G. R., et al.: Asian emissions in 2006 for the NASA
696 INTEX-B mission, *Atmos. Chem. Phys.*, 9, 5131–5153, doi:10.5194/acp-9-5131-2009,
697 2009b.

698 Zhao, C., Tie, X., Lin, Y.: A possible positive feedback of reduction of precipitation and increase
699 in aerosols over eastern central China, *Geophys. Res. Lett.*, 33(11), 2006.

700 Zhao, C., Liu, X., Leung, L. R., Johnson, B., MaFarlane, S. A., Gustafson, W. I., Fast, J. D.,
701 Easter, R.: The spatial distribution of mineral dust and its shortwave radiative forcing
702 over North Africa: modeling sensitivities to dust emissions and aerosol size treatments,
703 *Atmos. Chem. Phys.*, 11, 1879-1893, 2010.

704 Zhao, C., Liu, X., Leung, L. R., and Hagos, S.: Radiative impact of mineral dust on monsoon
705 precipitation variability over West Africa, *Atmos. Chem. Phys.*, 11, 1879-1893,
706 doi:10.5194/acp-11-1879-2011, 2011.

707 Zhao, C., Leung, L. R., Easter, R., Hand, J., and Avise, J.: Characterization of speciated aerosol
708 direct radiative forcing over California, *J. Geophys. Res.*, 118, 2372–2388,
709 doi:10.1029/2012JD018364, 2013a.

710 Zhao, C., Chen, S., Leung, L. R., Qian, Y., Kok, J., Zaveri, R., and Huang, J.: Uncertainty in
711 modeling dust mass balance and radiative forcing from size parameterization, *Atmos.*
712 *Chem. Phys.*, 13, 10733–10753, 2013b.

713 Zhong, S., and Yang, X. Q.: Ensemble simulations of the urban effect on a summer rainfall event
714 in the Great Beijing Metropolitan Area, *Atmos. Res.*, 153, 318-334. 2015a.

715 Zhong, S., and Yang, X. Q.: Mechanism of urbanization impact on a summer cold frontal rainfall
716 process in the Great Beijing Metropolitan Area, *J. Appl. Meteorol. Climatol.*, doi:
717 10.1175/JAMC-D-14-0264.1, 2015b.

718 Zhong, S., Qian, Y., Zhao, C., Leung, R., and Yang, X. Q.: A case study of urbanization impact
719 on summer precipitation in the Greater Beijing Metropolitan Area: Urban heat island
720 versus aerosol effects, *J. Geophys. Res. Atmos.*, 120, doi:10.1002/2015JD023753, 2015.

721

722

723

724

725

726

727

728 **Table and Figure Captions**

729 **Table 1** Configurations of the WRF physics schemes used in the present study.

730 **Table 2** Numerical experiments and corresponding urban land use and aerosol emissions.

731 **Table 3** Analysis strategies for the investigation of urban land-use and/or aerosol effects.

732 **Figure 1** Land-use categories for year (a) 1970; (b) 2006; and (c) SO₂ (units: mol km⁻² h⁻¹) and
733 (d) black carbon (BC) emission rates (units: ug m⁻² s⁻¹) averaged over 2006-2010. Surface
734 topography is also shown in Fig. 1a (contour; units: m). The boxes in Fig. 1b outline three mega-
735 city clusters of Nanjing, Su-Xi-Chang, and Shanghai.

736 **Figure 2** Moving spatial anomalies of averaged surface skin temperature (units: °C) with a
737 filtering window size of 1° × 1° for (a) MODIS observation and (b) the L06E06 simulation. The
738 “High Intensity Residential” and “Commercial/Industrial/Transportation” areas are marked with
739 green lines and yellow lines, respectively.

740 **Figure 3** Annual mean (a) near-surface temperature (units: °C) and (b) precipitation (units: mm
741 d⁻¹) from observations (shaded circles) and the LU06E06 simulation (shaded).

742 **Figure 4** Differences in mean 2-m temperature (Units: °C) between simulations (a, d) LU06E70
743 and LU70E70, (b, e) LU70E06 and LU70E70, (c, f) LU06E06 and LU70E70 for summer (upper
744 panels) and winter (bottom panels). “Commercial/Industrial/Transportation” areas are marked
745 with green lines. The black dots mark the area with statistically significant changes.

746 **Figure 5** Differences in net shortwave fluxes at the surface (units: W m^{-2}) between simulations
747 (a, c) LU06E70 and LU70E70, and (b, d) LU70E06 and LU70E70 in summer (upper panels) and
748 winter (bottom panels).

749 **Figure 6** Differences in column burden of PM_{2.5} (g m^{-2}) between simulations LU70E06 and
750 LU70E70, superimposed with near-surface winds simulated in LU70E70, for (a) summer and (b)
751 winter.

752 **Figure 7** Differences in mean summertime (a) heat wave days (units: d/yr) and (b) heat stress
753 (units: $^{\circ}\text{C}$) between simulations LU06E70 and LU70E70.

754 **Figure 8** Diurnal cycles of the frequency of summertime extreme rainfall events for LU70E70
755 (defined using hourly precipitation intensity above 95th percentile, black lines, right axis) and the
756 differences between simulations over (a) Nanjing, (b) Shanghai, and (c) Su-Xi-Chang. Red lines
757 are for Land use effect, blue lines for Aerosol effect, and green lines for the combined effect.

758 **Figure 9** Differences in the frequency of summertime extreme rainfall events (averaged from
759 12:00 to 20:00 LST) between simulations (a) LU06E70 and LU70E70, and (b) LU70E06 and
760 LU70E70.

761 **Figure 10** (a) Time-height cross-sections of differences (between LU06E70 and LU70E70) in
762 temperature (contour; units: $^{\circ}\text{C}$) and divergence (shade; units: 10^{-5} s^{-1}) averaged over the three
763 city clusters (Nanjing, Shanghai, and Su-Xi-Chang); (b) same as (a), but for vertical velocity
764 (shade; units: 10^{-2} m s^{-1}) and cloud water mixing ratio (contour; $10^{-3} \text{ kg kg}^{-1}$).

765 **Figure 11** Time-height cross-sections of differences between LU70E06 and LU70E70 in
766 radiative heating profile (shade; units: K d^{-1}), vertical velocity (contour; units: 10^{-2} m s^{-1}) and

767 surface solar radiation (blue bars; units: W m^{-2}) averaged over the three city clusters (Nanjing,
768 Shanghai, and Su-Xi-Chang).

769 **Figure 12** Rain rate (units: mm h^{-1}) superimposed with wind vectors at 850 hPa for case A from
770 08:00 LST 23 June to 08:00 LST 24 June 2006 (a) simulated in the LU06E06 simulation, (b)
771 differences between LU06E70 and LU70E70, (c) differences between LU70E06 and LU70E70.
772 Panels (d-f) are the same as (a-c) but for case B from 08:00 LST 1 July to 08:00 LST 2 July
773 2006. The boxes R1 in (a) and R2 in (d) outline the three regions over which further analysis are
774 conducted. Lines across the center of each box mark the cross-sections to be analyzed.

775 **Figure 13** The time evolution of precipitation (units: mm h^{-1}) along the line *ab* (marked in Fig.
776 12a) from 08:00 LST 23 June to 02:00 LST 24 June 2006 (case A) (a) simulated in the LU06E06
777 simulation, (b) differences between LU06E70 and LU70E70, (c) differences between LU70E06
778 and LU70E70. Panels (d-f) are the same as (a-c) but for case B along line *cd* (marked in Fig.
779 12d) from 08:00 LST 1 July to 02:00 LST 2 July 2006.

780 **Figure 14** The time-height cross-sections of differences in moisture flux convergence (shaded;
781 units: $10^{-4} \text{g}^{-1} \text{kg}^{-1} \text{s}^{-1}$) and water vapor mixing ratio (black lines; units: 10^{-2}g kg^{-1}) from 08:00
782 LST 23 June to 02:00 LST 24 June 2006 (case A) over region R1 (denoted in Fig. 12a) between
783 (a) LU06E70 and LU70E70; (b) LU70E06 and LU70E70; Panels (c, d) are the same as (a, b) but
784 for case B from 08:00 LST 1 July to 02:00 LST 2 July 2006 over R2 (denoted Fig. 12d).

785 **Figure 15** Same as Fig. 14 but for differences in the CON term (shaded; units: $10^{-4} \text{g}^{-1} \text{kg}^{-1} \text{s}^{-1}$)
786 and MA term (black lines; units: $10^{-4} \text{g}^{-1} \text{kg}^{-1} \text{s}^{-1}$) in eq. (2).

787 **Figure 16** Same as Fig. 15 but for differences in-the first term $(-V_{ctrl} \cdot \Delta(\nabla q))$ (shaded; units: 10^{-4}
788 $\text{g}^{-1} \text{kg}^{-1} \text{s}^{-1}$) and the second term $(-\nabla q)_{ctrl} \cdot \Delta V$ (black lines; units: $10^{-4} \text{g}^{-1} \text{kg}^{-1} \text{s}^{-1}$) in Eq.3.-